International Journal of Heat and Mass Transfer 52 (2009) 1138–1148

Contents lists available at ScienceDirect

International Journal of Heat and Mass Transfer

journal homepage: www.elsevier.com/locate/ijhmt

Heat transfer enhancement in self-sustained oscillatory flow in a grooved channel with oblique plates

Abdelkader Korichi [a,*], Lounes Oufer [b,1], Guillaume Polidori [c,2]

[a] Laboratoire de Mécanique, Physique et Modélisation Mathématique, Centre Universitaire de Médéa, Quartier Ain d'Heb, Médéa 26000, Algeria
[b] Université des Sciences et de la Technologie Houari Boumediene, Faculté de Génie Mécanique et de Génie des Procédés, Département de Génie Chimique et de Cryogénie, Laboratoire des Phénomènes de Transfert, BP 32, El-Alia, Bab-Ezzouar, Alger, Algeria
[c] Laboratoire de Thermomécanique, Faculté des Sciences, BP 1039, 51687 Reims, France

ARTICLE INFO

Article history:
Received 4 February 2008
Received in revised form 18 September 2008
Available online 14 November 2008

Keywords:
Heated obstacle
Heat transfer enhancement
Oscillatory flow
Oblique plate

ABSTRACT

The aim of this work is to investigate the conjugate heat transfer in periodic mounted obstacles channel with oblique plates as vortex generators installed at the rear obstacles on the opposite wall. Special attention will be paid to the analysis of flow evolution and heat transfer enhancement in the intermediate and low Reynolds number range without recourse to turbulent flow. Various physical arrangements are considered as plate length, tilt angle and Reynolds number in order to investigate their influence on the thermal and flow characteristics in the steady state as well as in the self-sustained oscillatory flow.

1. Introduction

Transitional flow regimes in channel with geometrical inhomogeneities, are of great importance in numerous engineering fields, such as compact heat exchangers, oxygenators and, dialysers and electronic cooling systems of electronic equipment. A significant research effort has been devoted to finding the best ways to study these flow regimes and many techniques based on both active and passive methods have been proposed to enhance heat transfer in these applications. Among these methods one can find systems involving vortex generators such as fins, ribs and other cylinders. The geometrical characteristics of vortex generators play a significant role in the rate of heat transfer. Disturbance promoters increase fluid mixing and interrupt the development of the thermal boundary layer, leading to enhancement of heat transfer. However, the complex flow characterized by the appearance of successive separations, recirculation, reattachment and deflection make the understanding of the flow behaviour and the evolution of heat transfer in such systems more difficult.

Wu and Perng [1] investigated the effect of installing an oblique plate on heat transfer over an array of five obstacles mounted in a horizontal channel and they observed an enhancement of heat transfer of up to 39.5% in the value of *Nusselt* number.

Garimella and Eibeck [2] experimentally investigated the effect of prostration of a vortex generator on heat transfer from an array of discrete heat sources. A maximum heat transfer enhancement of about 40% was reported.

In a study by Herman and Kang [3], the effect of setting curved vanes in a grooved channel was investigated. Enhancement of heat transfer was then reached with rates similar to those obtained in turbulent flow although at low Reynolds numbers. This enhancement of heat transfer was mainly the result of fluid flow acceleration between the vane and the heated block and the elimination of large recirculation regions within the grooves. Yang [4] proposed an oscillating bar as a vortex generator in a channel with heated obstacles. His results showed that the vortices induced by the oscillating bar allowed an increase in heat transfer from the heated obstacles. Fu and Tong [5] carried out a numerical simulation on the effect of an oscillating cylinder on the heat transfer from heated blocks in a channel flow. Their results proved that heat transfer was remarkably enhanced as the oscillating frequency of the cylinder was in the lock-in region. Ko and Anand [6] reported an experimental investigation about heat transfer and pressure drop in a uniformly heated rectangular channel with wall-mounted porous baffles. Their findings showed that the use of such material could enhance heat transfer rates by up to 300% when compared to smooth heated channels. However, this heat transfer enhancement was accompanied by a significant increase in

* Corresponding author. Tel./fax: +213 25 58 28 10.
E-mail addresses: ab_korichi@yahoo.fr (A. Korichi), lounesoufer@yahoo.fr (L. Oufer), guillaume.polidori@univ-reims.fr (G. Polidori).
[1] Tel./fax: +213 21 24 71 69.
[2] Tel./fax: +33 3 26 91 32 73.

0017-9310/$ - see front matter © 2008 Elsevier Ltd. All rights reserved.
doi:10.1016/j.ijheatmasstransfer.2008.09.013

Nomenclature

A	dimensionless surface area
d	plate length
h	dimensionless obstacle height ($=h^*/H$)
H	channel height
k	thermal conductivity
L	dimensionless obstacle spacing ($=L^*/H$)
Nu	*Nusselt* number
$Nu_{\text{face i}}$	mean face *Nusselt* number
Nu_{overall}	overall obstacle *Nusselt* number
Nu_x	local *Nusselt* number
p	dimensionless pressure
Pe	*Peclet* number
Pr	*Prandtl* number
Re	*Reynolds* number
T	temperature
t	time
u and v	dimensionless velocity components
w	dimensionless obstacle width ($=w^*/H$)
x and y	dimensionless coordinates

Greek symbols

α	thermal diffusivity
β	linear part in pressure function of Eq. (10)
γ	plate angle
Δ	difference
θ	dimensionless temperature
ν	kinematic viscosity
ρ	density
τ	dimensionless time

Subscripts

b	bulk
f	fluid
m	mean
p	refers to one period
s	solid
w	wall
0	at inlet conditions

Superscript

$*$	dimensional

Other

–	time average

pressure drop. Self-sustained oscillatory flow has been widely investigated by Amon et al. [7] and Nigen and Amon [8]. They determined that the laminar flow undergoes a flow bifurcation at a critical Reynolds number which is significantly lower than the one related to a Poiseuille plane channel flow. These investigations indicated that the heat transfer rate increases when the flow passes from a laminar to a transitional regime, which is due to better flow mixing after flow bifurcation, and also that this enhancement is usually accompanied by an increase in the pressure drop.

Nishimura et al. [9] experimentally investigated the influence of the imposed oscillatory frequency on mass transfer enhancement of grooved channels with different cavity lengths, for an external pulsatile flow. It was found that the mass transfer enhancement by means of fluid oscillations is higher in laminar than in turbulent flow and there is noticeable enhancement at intermediate Strouhal numbers, depending on the cavity length and Reynolds number. Adachi and Uehera [10] performed numerical investigations of flow and temperature fields for steady state and self-sustained oscillatory flows in periodically grooved channels for various channel geometrical configurations. They determined correlations existing between heat transfer and pressure drops and they found that heat transfer is significantly enhanced, and pressure drop increases after the first flow bifurcation. They found that the bifurcation occurs at *Reynolds* number in the range of 1000–1100. They also determined that expanded grooved channels perform more efficiently than contracted grooved ones. Recently, Guzmán and Del Valle [11] performed numerical investigations of the transition scenarios and heat transfer characteristics in grooved channels as the flow regime evolves from a laminar to a transitional regime. They found that the mean heat transfer rate remains mostly constant in the laminar steady regime but it continuously increases in the case of transitional regime. The rate of increase of this heat transfer is higher when the flow regime is quasi-periodic rather than periodic. This enhancement is twice more important in the periodic flow regime and it can be twice and half higher for the quasi-periodic regime. Wang and Jaluria [12] numerically studied heat transfer enhancement by using a square cylinder as vortex generator in the upstream obstacles channel at low Reynolds number. They found that heat transfer can enhance up 95% for Reynolds number of 1000. Self-sustained oscillatory flow in a grooved channel was also studied in heat transfer and fluid mixing by several researchers [13,14].

This study lies within the scope of previous works and focuses the way to investigate the conjugate heat transfer in periodic mounted obstacles channel with oblique plate as vortex generator installed at the rear obstacles on the opposite wall. This way to improve heat transfer by modifying the direction of the flow towards the obstacle faces and by activating the self-oscillations using oblique plates placed periodically can be considered as a new approach and be used in the cooling air of electronic systems. Special attention will be paid to the analysis of flow evolution and heat transfer enhancement in the intermediate and low Reynolds number range without recourse to turbulent flow. The study is limited to Re = 1000 because methods of cooling electronic components in laminar forced convection usually concern velocities ranging from 0.3 to 5 m/s (Anderson and Moffat [15]). This corresponds to a Reynolds number based on the hydraulic diameter ($d_h = 2H$) varying from 200 to 2000 or $Re_H = 100$–1000. Various physical arrangements are considered as plate length, plate tilt angle and Reynolds number in order to investigate their influence on the thermal and flow characteristics in the steady state as well as in the self-sustained oscillatory flow.

2. Mathematical formulation

Fig. 1 shows the physical geometry considered in this study. It consists of a two-dimensional horizontal channel containing heating blocks regularly distributed on its lower wall and insulated oblique plates of low thickness (thickness/H = 0.01) at the upper wall. Each block base is maintained at a constant temperature. The flow is assumed to be laminar and incompressible, the fluid viscous Newtonian. Buoyancy induced effects are negligible based on typical experimental and numerical calculation in similar configurations [11]. All the physical properties of the fluid and of the solid are considered as constant. The formulation adopted here is that of a constant flow rate in time with a fluctuating pressure gradient between the inlet and the outlet of each module. The imposed nondimensional flow rate value is given by $u_{0m} \cdot H = 8/3$.

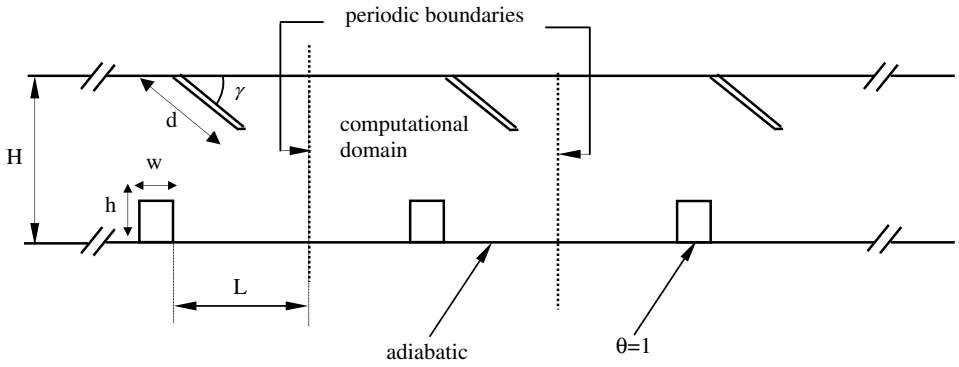

Fig. 1. Schematic diagram of computational domain and boundary conditions.

Buoyancy effects are neglected with respect to the forced convection effects because of the low difference of temperature which is assumed. The *Prandtl* number is taken equal to 0.71. The dimensionless groups defined in the nomenclature are used to express the governing transport time-dependent equations in the dimensionless form. The following non-dimensional variables have been defined:

$$u=\frac{u^*}{u_0},\quad v=\frac{v^*}{u_0},\quad x=\frac{x^*}{H},\quad y=\frac{y^*}{H},\quad \tau=tu_{0m}/H$$
$$p=\frac{p^*}{\rho u_{0m}^2},\quad \theta=\frac{T-T_0}{T_w-T_0};\quad \mathrm{Re}=\frac{\rho u_{0m}H}{\mu};\quad Pe=\mathrm{Re}\cdot\mathrm{Pr} \qquad (1)$$
$$\text{and},\quad \alpha=\frac{k}{\rho C_p}$$

where, u^* and v^* are the velocity components, p^* the pressure, ρ the density, T the temperature, H the channel height, u_{0m} the mean velocity at the inlet conditions, k_f the fluid thermal conductivity and α_s and α_f are the thermal diffusivities of the solid and fluid phase, respectively. The subscripts "0" and "w" are related to the inlet condition and wall, respectively.

The resulting non-dimensional equations for mass, momentum and energy conservation are presented in the Cartesian coordinate system as follows:

Mass:

$$\frac{\partial u}{\partial x}+\frac{\partial v}{\partial y}=0 \qquad (2)$$

with (u,v) and (x,y) the dimensionless velocity components and coordinates, respectively.

X-momentum:

$$\frac{\partial u}{\partial \tau}+u\frac{\partial u}{\partial x}+v\frac{\partial u}{\partial y}=-\frac{\partial p}{\partial x}+\frac{1}{\mathrm{Re}}\left(\frac{\partial^2 u}{\partial x^2}+\frac{\partial^2 u}{\partial y^2}\right) \qquad (3)$$

Y-momentum:

$$\frac{\partial v}{\partial \tau}+u\frac{\partial v}{\partial x}+v\frac{\partial v}{\partial y}=-\frac{\partial p}{\partial y}+\frac{1}{\mathrm{Re}}\left(\frac{\partial^2 v}{\partial x^2}+\frac{\partial^2 v}{\partial y^2}\right) \qquad (4)$$

Energy:

For the fluid phase:

$$\frac{\partial \theta_f}{\partial \tau}+u\frac{\partial \theta_f}{\partial x}+v\frac{\partial \theta_f}{\partial y}=\frac{1}{Pe}\left(\frac{\partial^2 \theta_f}{\partial x^2}+\frac{\partial^2 \theta_f}{\partial y^2}\right) \qquad (5)$$

For the solid phase:

$$\frac{\partial \theta_s}{\partial \tau}=\alpha_s\left(\frac{\partial^2 \theta_s}{\partial x^2}+\frac{\partial^2 \theta_s}{\partial y^2}\right) \qquad (6)$$

2.1. Boundary conditions

In channel with a periodic geometry and after a short entrance region, the flow is expected to reach a periodically fully developed regime in which the velocity field repeats itself from any module to another. However the number of modules that constitute the period depends on both the Reynolds number and the geometrical configuration. The use of periodic boundary condition has been first introduced by Patankar et al. [16] where only one module was considered. Later, the assessment of the periodicity of the flow was studied by many researchers. Using the linear stability theory, Adachi and Uehara [17] and Adachi and Hasegawa [18] found that the flow repeat periodically every two modules, for the unsteady regime and for a channel blockage ratio of 0.5. However, other studies have considered one module for similar conditions [10,19,20].

For similar conditions to our study and using a numerical simulation, Young and Vafai [21] found that the periodicity of the mean Nusselt number is established, relatively to the ninth obstacle, at the 5% and 10% difference levels (eighth and seventh obstacles, respectively). The periodic behaviour of the velocity components and temperature distributions are also explicitly demonstrated for the array.

For a similar geometry, experimental studies reported by Garimella and Eibeck [2] and Jubran et al. [22] demonstrate that the results do not depend any longer on the obstacle number after the third to the fourth obstacle. Another relevant study about the assessment of periodic boundary conditions shows that the flow can become periodic around the fifth groove for a blockage of 0.5 [23]. Greiner [24] showed that the flow was hydro-dynamically periodically and fully developed after the seventh or eighth rib. One can notice that Guzmán and Del Valle [11] have also investigated the existence of a fully developed periodic flow for a similar configuration. Lorenz et al. [25] found that the flow is thermally periodic in a grooved channel, after the fifth rib for a blockage ratio of 1/3. Habib et al. [26] from an experimental investigation in baffled channel, found that the flow reaches a periodic state from one module to another, after the second module and for a blockage ratio of 0.5. In the study of Grosse-Gorgemann et al. [27], the Strouhal number obtained by numerical calculation using the periodic boundary conditions is the same as that obtained in experiments for a baffled channel at blockage ratio of 0.5.

From these previous studies and for the present configuration (blockage ration equal to 0.5 and $Re \leqslant 1000$), we can assume that the flow is periodic from one module to another.

Introducing the L dimensionless obstacle spacing ($=L^*/H$), the dimensionless velocity components, temperature and pressure are such that:

$$u(x+L,y,t)=u(x,y,t);\ v(x+L,y,t)=v(x,y,t) \tag{7}$$

$$\frac{\theta(x+L,y,t)-\theta_w}{\theta_b(x+L)-\theta_w}=\frac{\theta(x,x,t)-\theta_w}{\theta_b(x)-\theta_w} \tag{8}$$

where, $\theta_b(x,t)$ is the cross-sectional local bulk temperature defined by:

$$\theta_b(x,t)=\frac{\int_0^H |u(x,y,t)|.\theta(x,y,t)dy}{\int_0^H |u(x,y,t)|dy} \tag{9}$$

$$p(x+L,y,t)=p(x,y,t)+\beta \tag{10}$$

where, $\beta=(t)$ is the linearly-varying component of the dimensionless pressure which results in a force acting on the fluid in the momentum equations and is adjusted every time at each step to satisfy the fixed mass flow rate condition. The reason why the absolute value of the velocity is used is that in such a way regions with reverse flow are properly represented [10,16]. The integrals can be used over the entire cross-sectional area of the channel.

At the channel walls ($y=0, y=1$), the no-slip condition is assumed, that is $u=v=0$. For the thermal boundary conditions, the walls and the oblique plate surface are assumed to be insulated except at the obstacle bases where a constant temperature is imposed ($\theta=1$). At the solid–fluid interface, continuity of both heat flux and temperature is also supposed to hold on.

3. Numerical solution

The governing transport equations associated with the boundary conditions are solved by using the finite volume formulation. The SIMPLER algorithm developed by Patankar [28] is adopted. The time discretization scheme is implicit with second order accuracy. For the spatial discretization, the central second order differencing scheme is used for the diffusive terms and the QUICK scheme is used for the convective terms. The iterative solution is continued until the residuals for all computational cells become less than 10^{-6} for all dependent variables. Calculation is continued until both the velocity components and the temperature at the exit module ($x=0.375, y=0.5$) become independent from time for the steady state or periodic in time for the self-sustained oscillatory flow.

For all the calculations performed, a fine grid of 150×200 control volume was found to be sufficient for the range of *Reynolds* numbers investigated. The equally spaced grid system is used because the onset travelling waves engender moving high pressure and velocity gradients in the computational domain. Moreover, the displacement of these waves over the coarser mesh results in higher calculation errors in this zone. In order to check grid independence, numerical simulations of the unsteady problem are performed with various grid sizes. For the three 150×100, 150×200 and 200×300 grid sizes and for $Re=250$ and 1000, it is found that the maximum relative error for global parameters such as mean *Nusselt* number is only 3%. The calculations of marching time are started with the fluid at rest and a small dimensionless time step $\Delta\tau=2\times10^{-5}$ to 0.001, dependent on the configuration and Reynolds number is considered in order to capture the complex unsteady flow. Finally and in order to take in account the conjugate heat transfer, the treatment of the sudden changes of the thermophysical properties at the solid–fluid interface is handled by applying the domain extension method the details of which are presented in [29]. The code was already validated and used in previous works [30–33]. It is important to note that 300,000 time steps are needed to obtain fully developed time periodic flow at $Re=1000$ which takes about 210 hours for $\Delta\tau=2\times10^{-5}$, on a PC with P4 processor. However, it has to be noted that the development of the thermal field takes even more time.

4. Results and discussion

The dimensionless parameters having to be considered and which characterize the flow field and heat transfer are as follows: The *Reynolds* number based on channel height is taken equal to 250, 600 and 1000, the obstacle dimensions ($h=h^*/H; w=w^*/H$) and the obstacle stream-wise spacing (L) are taken as $h=w=0.25$ and $L=0.5$. With respect to the plaque length (d) and tilt angle (γ) four configurations are tested as indicated in Table 1. At last, the solid to fluid thermal conductivity ratio is taken equal to 10.

In order to take better advantage of the obtained results, the following definitions are to be specified:

Local *Nusselt* number defined by the local temperature gradient at the wall:

$$Nu_x=-\frac{\partial\theta}{\partial n}\Big|_{blocksurface} \tag{11}$$

where, n denotes normal to the solid surface and the temperature gradient at the wall is calculated using a three-point finite difference.

Time-averaged local *Nusselt* number by period (the subscript "*p*" *refers to one period*):

$$\overline{Nu_x}=\frac{1}{\tau_p}\int_0^{\tau_p} Nu_x d\tau \tag{12}$$

Mean face *Nusselt* number:

$$Nu_{face\ i}=\frac{1}{A_{face\ i}}\int_{face\ i} Nu_x dl \tag{13}$$

where A_{face} is the exposed obstacle face area (vertical or horizontal faces) and dl is equal to dx for the horizontal face and dy for the vertical faces.

Time-averaged face *Nusselt* number:

$$\overline{Nu_{face}}=\frac{1}{\tau_p}\int_0^{\tau_p} Nu_{face} d\tau \tag{14}$$

Overall obstacle *Nusselt* number:

$$Nu_{overall}=\frac{\sum_{face1}^{face3} A_{facei} Nu_{facei}}{A_{face1}+A_{face2}+A_{face3}} \tag{15}$$

where $Nu_{face\ i}$ is the mean face *Nusselt* number.

Time-averaged overall *Nusselt* number around a heated obstacle:

$$\overline{Nu_{overall}}=\frac{1}{\tau_p}\int_0^{\tau_p} Nu_{overall} d\tau \tag{16}$$

Global conjugate heat transfer in complex geometries such as electronic systems strongly depends on the local flow structure and therefore relies on the prediction of the local flow pattern. In such systems, the low velocities and small length scales correspond to low *Reynolds* number, hence leading to laminar flow characterized by complex structures such as separation, reattachment and recirculation. This makes an accurate determination of the distribution of the local convective heat transfer a difficult task. The following section is devoted to understanding the flow behaviour before analysis of heat transfer is undertaken.

Table 1
Geometric parameters for the four cases studied.

Case	d	γ (°)
1	0.25	45
2	0.32	45
3	0.25	60
4	0.32	60

4.1. Flow structure

Flow in channel with singularities like grooved channel, bifurcates to unsteady flow at critical Reynolds value before bifurcation to turbulent flows. However, the critical Reynolds number values for the basic grooved channel (BGC) is relatively high, as demonstrated in [3].

From Fig. 2 we can show the behaviour of the longitudinal velocity component as a function of time for $Re = 1000$ for the BGC and for $Re = 250$ for the grooved channel with oblique plates (GCOP), at the reference point ($x = 0.75, y = 0.25$). At low *Reynolds* number ($Re < Re_c$) the histogram indicates a constantly decaying amplitude to reach the steady-state flow. For the GCOP, the critical Reynolds number (Re_c) is much lower than the one for the BGC. Although, the precise determination of this parameter (Re_c) is not considered in this study, it seems that Re_c is highly dependent on plate length and tilt angle. Among the four configurations studied here, only the forth case is shown to induce a value of Re_c below 250. An example of the flow structure for this steady state flow condition obtained for the BGC is illustrated by Fig. 3a. This figure shows that the flow pattern is characterized by parallel streamlines in the mid-section and a large stationary vortex occupies the whole grooved region between blocks. For steady state flow, the main difference between the flow structures in BGC and GCOP is the stationary vortex upstream and downstream of the oblique plate (Fig. 3b). Even if Fig. 3 seems to indicate that the obstacles on the upper and lower walls affect streamlines independently at $Re = 250$, it is not the case at high Reynolds numbers. Indeed, for $Re > Re_c$, the flow regime becomes periodic (self-oscillations) so that the structure of the flow is totally different in comparison with the case without a plate. Moreover with the presence of a plate at the top, the critical Reynolds number value varies considerably (ratio one to three or even more). At higher Reynolds number ($Re > Re_c$), increasing time, the velocities histogram at the reference point is converged asymptotically to a periodic state with fixed oscillatory amplitude as shown in Fig. 4. This flow oscillation is induced by the onset of Tollmien–Schlichting (T–S) waves activated by Kelvin–Helmholtz shear-layer instabilities spanning the groove caused by the periodic compression expansion due to the geometric topology.

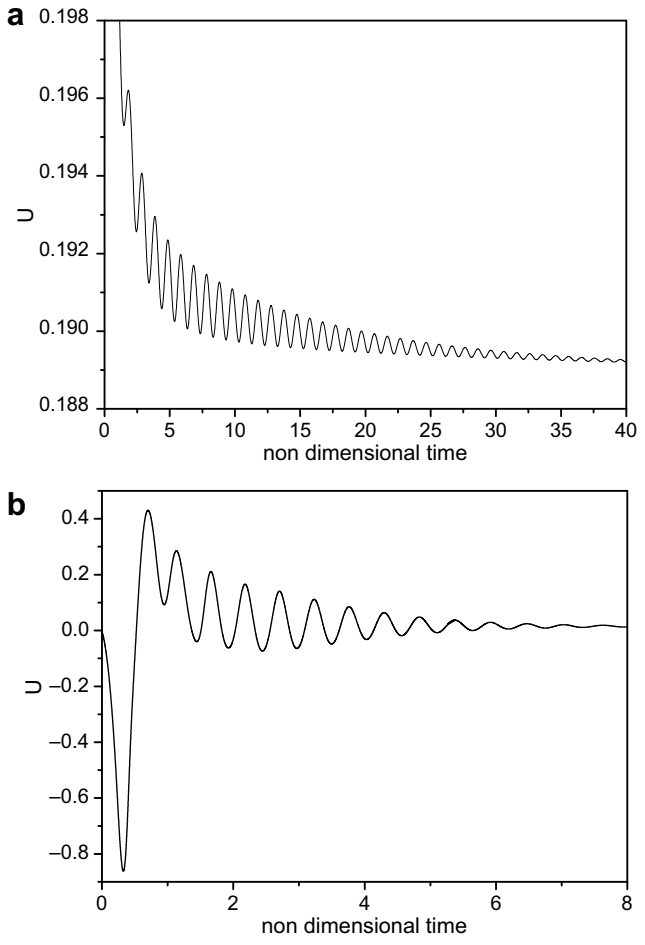

Fig. 2. u-velocity component history at the reference point ($x = 0.75, y = 0.25$): (a) for the BGC case and $Re = 1000$, (b) for the GCOP case 1 and $Re = 250$.

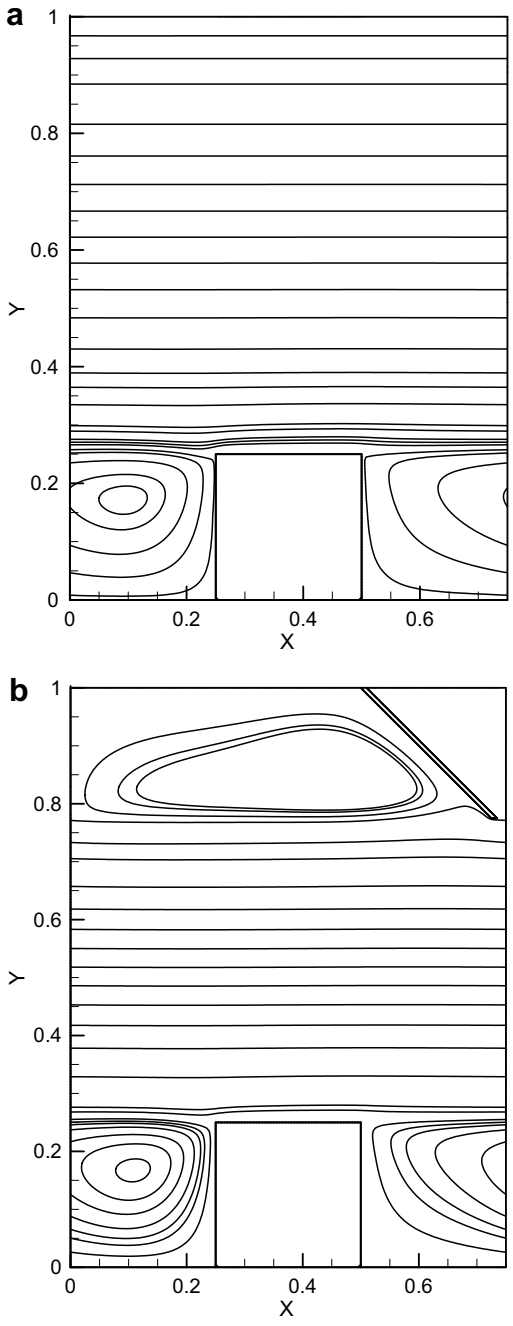

Fig. 3. Streamlines pattern for $Re = 250$: (a) for the BGC and (b) for the GCOP case 1.

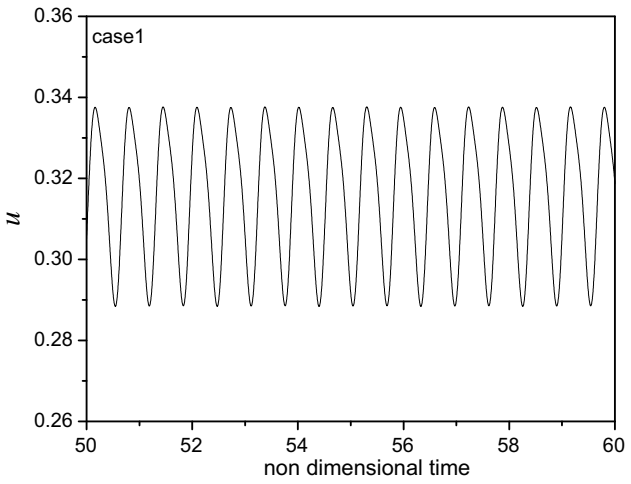

Fig. 4. Time history of the u-velocity component at the reference point ($x = 0.75, y = 0.25$) for case 1 at $Re = 600$.

To understand more about flow structure behaviour in the self-sustained oscillatory flow, Fig. 5 shows a sequence of six instantaneous streamline patterns during one time period for a periodic transitional Reynolds number of $Re = 600$ for case 4. These sequences demonstrate the wavy periodic nature of the flow as it moves downstream, and show a flow pattern of several vortices of different sizes, which increase and decrease in size. As explained later, this phenomenon ejects the fluid from the cavity to the main flow. In this section, only the flow behaviour of the flow in vicinity of a lower wall is explained. First (Fig. 5a), a deflection of the flow happens in the groove along the trailing edge of the obstacle caused by high pressure which prevails above this same edge. After a while, the flow deflection penetrates more deeply and reaches the bottom channel wall (Fig. 5c). As this deflection moves downstream, a vortex is generated from the trailing edge of the obstacle (Fig. 5d). After that, the later vortex grows downstream until it contacts the front face of the obstacle in subsequent module which is similar to the upstream obstacle in the actual module (Fig. 5d–f). This vortex grows up in space and intensity and occupies the whole inter-obstacle cavity; its height exceeds the height of the obstacle. The sequence is repeated periodically in time.

The Fast Fourier Transform (FFT) of the u-component time evolution for the four configurations is plotted in Fig. 6 at the same Reynolds value. For case 1, one can see a dominant fundamental frequency and a harmonic with low amplitude. This corresponds to the superposition of two waves which obviously result from the u-velocity histogram (not presented for conciseness). Two harmonics can be distinguished for cases 2 and 3 (Fig. 6b and c). The amplitude of the first harmonic is obvious on the right hand of the fundamental frequency. Finally, two harmonics with low

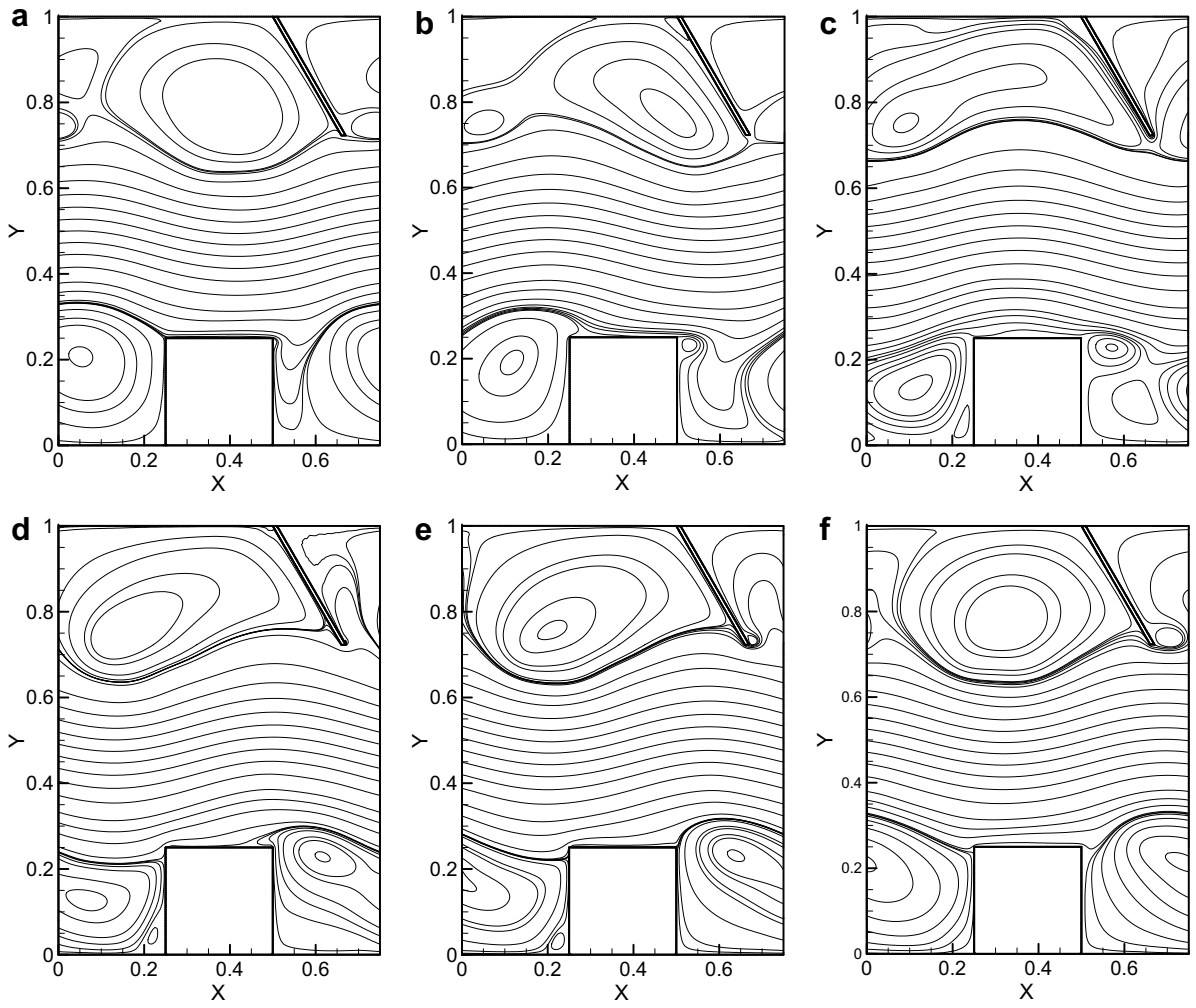

Fig. 5. Streamlines for seven time intervals of period of oscillation for case 4 at $Re = 600$: (a) = 5.790, (b) = ,5.872, (c) = 5.952, (d) = 6.032, (e) = 6.072, and (f) = 6.132.

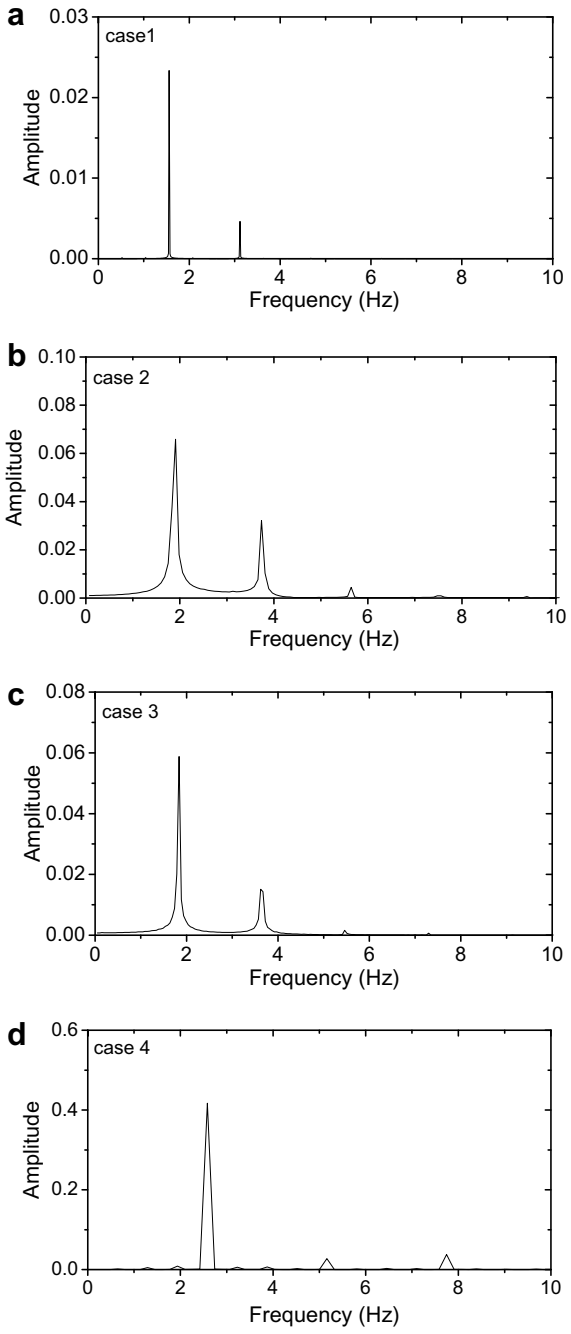

Fig. 6. FFT analysis of the u-velocity component history for $Re = 600$: (a) case 1, (b) case 2, (c) case 3, and (d) case 4.

amplitude can be seen (Fig. 6d). It should be noted that for each case the harmonics frequencies are a linear combination of the fundamental frequency $f_i = i \cdot f_0$, where f_0 is the fundamental frequency and i is the harmonic order. Table 2 summarises the fundamental frequencies and the corresponding periods of oscillation for the four cases studied. That leads to the conclusion that the frequency of oscillation increases at the same rhythm as the obstruction aspect ratio (in addition, the periodic behaviour has also been confirmed by the well-closed loop of the Lissajous's phase diagram).

Table 2
Fundamental frequencies and the corresponding period for the four cases.

Case	f	τ_p
1	1.558	0.641
2	1.907	0.524
3	1.836	0.545
4	2.582	0.387

4.2. Thermal field

In this section are presented detailed thorough analyses of temperature field and heat transfer results for the cases examined in Table 1. The time averaged value is used when the field is time periodic. Fig. 7a shows an illustrative sample of isotherms contours for the BGC at $Re = 250$, the results being similar to those obtained in the course of previous investigations by other searchers. As shown in this figure, above the horizontal obstacle face the

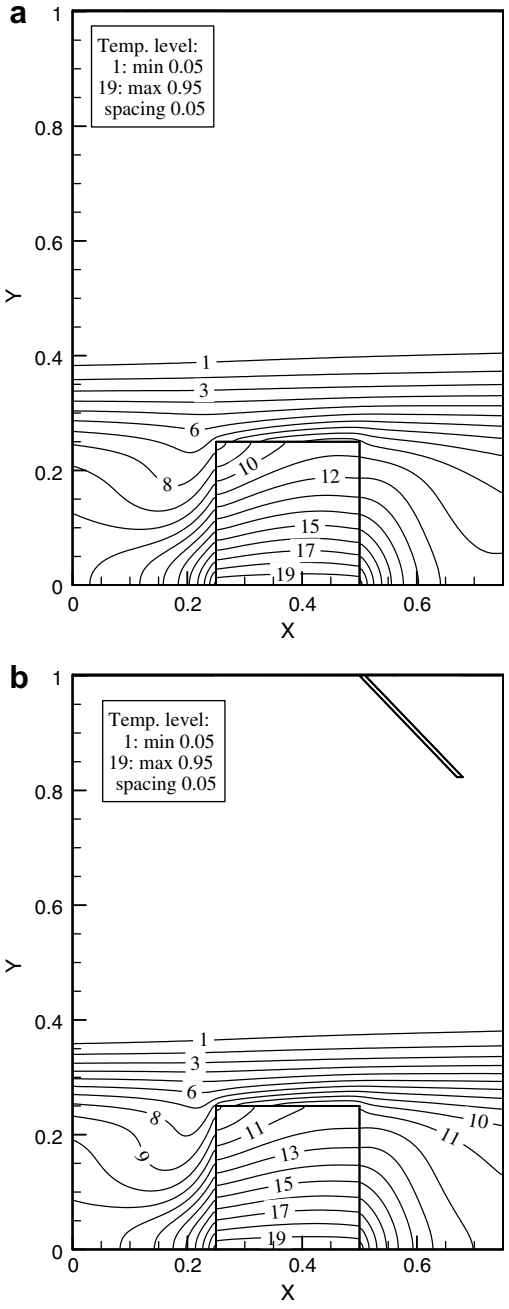

Fig. 7. Isotherms at $Re = 250$, (a) for the BGC and (b) for the GCOP.

isotherms are almost parallels with a slight slop toward the downstream channel, because the fluid temperature rises with removing energy as the fluid moves downstream. Under the steady state flow condition, the isotherms contours in the GCOP are quasi-similar to those obtained for the BGC, except for some difference in the temperature gradient (see Fig. 7b). At this flow regime, diffusion is the main heat transfer mechanism in the groove because of the poor mixing of the vortex in the groove with the main flow. The temperature distribution presents some stratification in both solid and fluid phases, a phenomenon also observed [11].

In the GCOP, at higher Reynolds number, i.e. $Re > Re_c$, the isotherms contours underline the wavy nature and vortex dynamic of the oscillatory flow. Fig. 8 shows sequences of instantaneous isotherms for the six time intervals corresponding to the flow field presented in Fig. 5. In order to easily understand the thermal-flow interaction, are presented in the same figure both the isotherms contours and some streamlines in the sensible zones. First, the warm fluid is carried out away and ejected into the main flow by the clockwise vortex situated downstream the obstacle, (Fig. 8a). At this time the thermal boundary layer on the left upper obstacle is very thin and develops along the horizontal face. Next, as the vortex grows in size and strength, the warm fluid is visible as a plume at the inlet module (at the left of the obstacle) (Fig. 8b). The vortex part on the upstream obstacle pulls down the cold fluid into the groove. The thermal boundary layer on the horizontal obstacle face is compressed. When the vortex is shed at the right upper corner of the obstacle, the isotherms above tend to deflect and then these isotherms present a concavity in the neighbourhood of the same corner. As the last vortex grows and moves downstream (Fig. 8c), the warm fluid passes over the obstacle face, rolls up and starts moving toward the main stream channel. Under the effect of the fast core flow, a hot fluid zone gets detached and moves with core flow above the obstacle. The cold fluid penetrates more into the groove and takes more space until the exit of the upstream module. Fig. 8d–f show that the isotherms go on moving up from the warm fluid into the groove near the obstacle corner. At the top obstacle face, the thermal boundary is agitated and disturbed with flow oscillation. Unfortunately, because the working fluid is air ($Pr < 1$), the boundary layer for the velocity becomes thinner than that for the temperature. Consequently, this leads to an increase of pressure drop penalty more than heat transfer enhancement near the obstacles. This increase of pressure drop is mainly due to the significant blockage ratio and to flow distortion. One can note that this increase can reach a drastic value at high blockage ratio ($d = 0.32, \gamma = 60°$). The flow velocity linearly increases with increasing the blockage ratio, and the pressure drop is observed to be proportional to the square of the velocity.

During the whole cycle, the isotherms imitate the oscillatory flow behaviour.

In terms of *Nusselt* number by face, at steady state flow, i.e. $Re < Re_c$, the *Nusselt* number presents an enhancement about 46% for cases 1–3 for the GCOP compared to the BGC at the frontal face

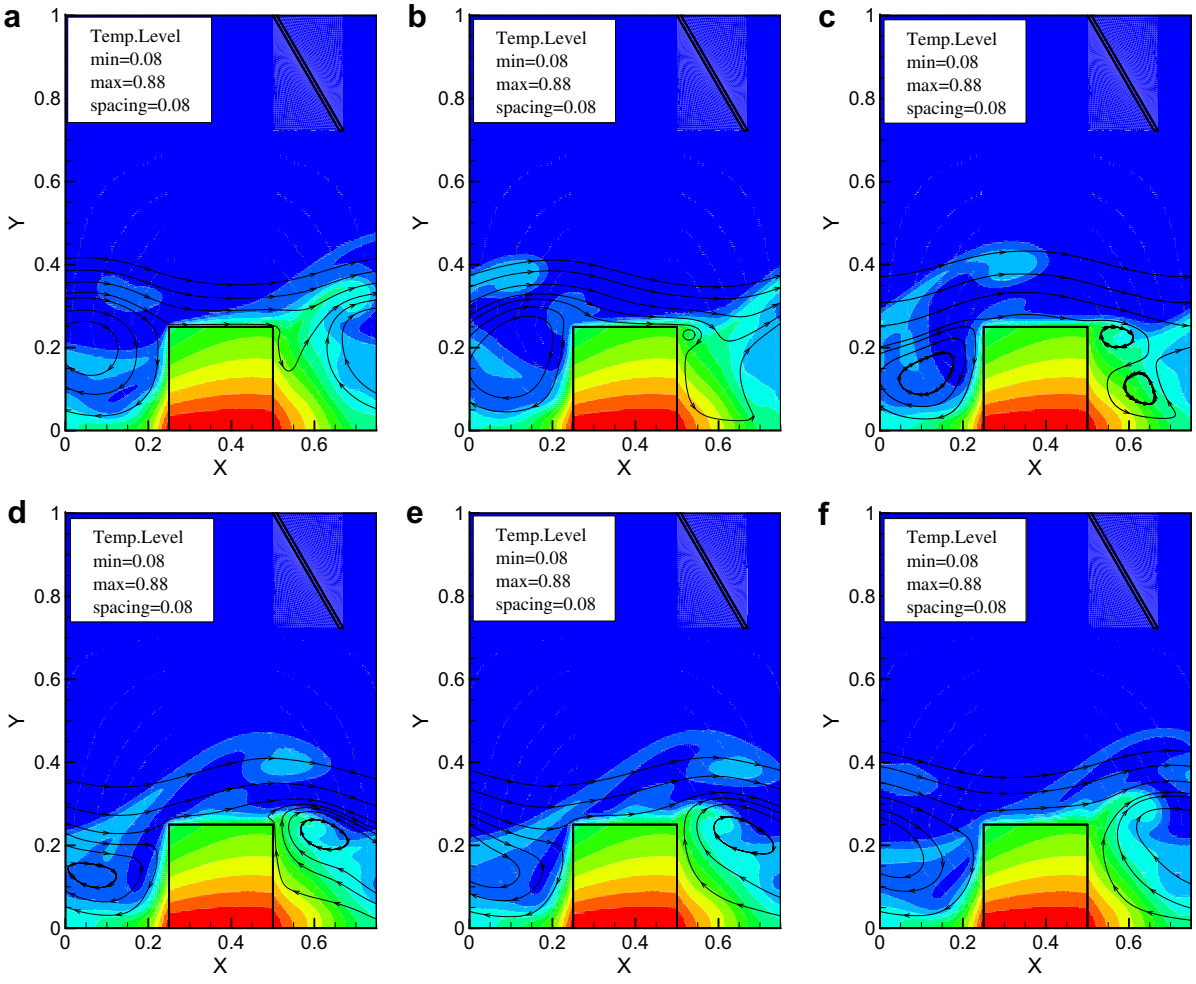

Fig. 8. Instantaneous isotherms for seven time intervals of period of oscillation for case 4 at $Re = 600$: (a) = 5.790, (b) = ,5.872, (c) = 5.952, (d) = 6.032, (e) = 6.072, (f) = 6.132.

(called face 1), (Fig. 9a). From this figure, we can see that the enhancement is more important, up to 123% for case 4 for the same face, where the flow is already unsteady at the same Reynolds number. For the horizontal face (called face 2), the enhancement is more important because this benefits from the flow redirection by the plate. For the rear face (face 3), no enhancement was observed, except an enhancement of 45% for case 4. For higher Reynolds number ($Re = 600$), a considerable enhancement was observed along the frontal and horizontal faces for all the cases. However, along the rear face, the enhancement was observed only for the first case. This later configuration allows equitable enhancement for the three exposed faces which avoids excessive temperature elevation: that is an important criterion in thermal management of electronic cooling industry. Increasing the Reynolds number (Fig. 9c) leads to similar trends for frontal and horizontal faces while the higher enhancement the case 2. It is noticed that case 4 is not plotted in Fig. 9c because the present study concerns only periodic regime. From this $Re = 1000$, the flow regime is seen to evolve towards a chaotic behaviour.

The obstacle mean *Nusselt* number versus Reynolds number for the five cases is plotted in Fig. 10. From this figure, it can be deduced that considerable enhancement in obstacle mean *Nusselt* number is obtained at the unsteady flow regime for all the cases. For low plate length ($d = 0.25$), the plate angle has no effect in the obstacle mean *Nusselt* number, however for a high value of the length ($d = 0.32$), the obstacle mean *Nusselt* number increases drastically with an increasing plate tilt angle. Because of the strength flow impact on the horizontal face (face 2) which contributes largely to removing heat from it. The global heat transfer enhancement observed for the GCOP compared to the BGC for different Reynolds number is reported in Table 3. The maximum heat transfer enhancement is obtained for case 4; however this enhancement is produced principally at the horizontal face. The heat transfer enhancement in the steady state flow is below 50% for all the cases, but this rate is over 75% at the self-sustained oscillatory flow. The maximum heat transfer enhancement is nearly 200% and obtained for the forth case at $Re = 600$ but as expected this rate is obtained only for the frontal and the horizontal faces. The optimal distribution of heat transfer enhancement is obtained for the first case at $Re = 600$. The best enhancement on the rear face is obtained for the case 1 at $Re = 600$, even if this is not the highest Reynolds number; it is due to the fact that the thermal transport from the rear face is dominated by the recirculation flows. These vortices are recirculation regions that trap the flow and lead to long residence times for fluid particles. For this case and for highest Reynolds number, e.g. $Re = 1000$, the vortex shed from the upper right corner, during the cycle oscillation, is large enough to affect a larger surface (Fig. 11a and b). Similar finding was reported by

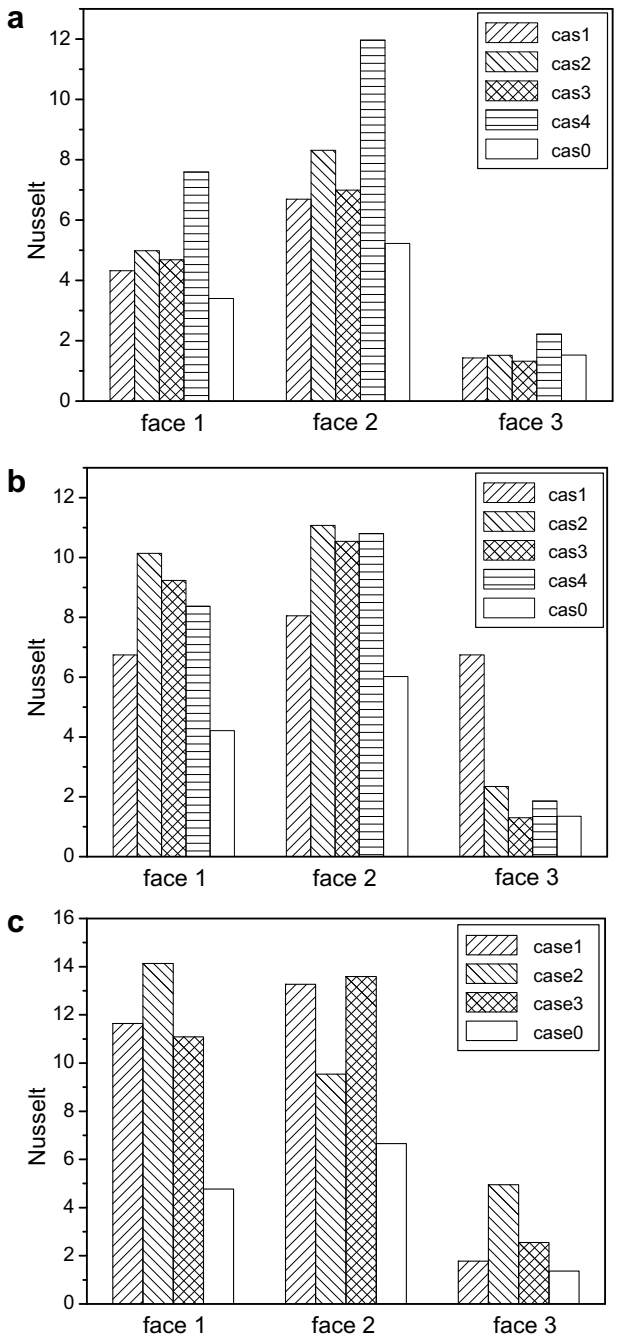

Fig. 9. Mean *Nusselt* number by face for the five cases: (a) $Re = 250$, (b) $Re = 600$, and (c) $Re = 1000$.

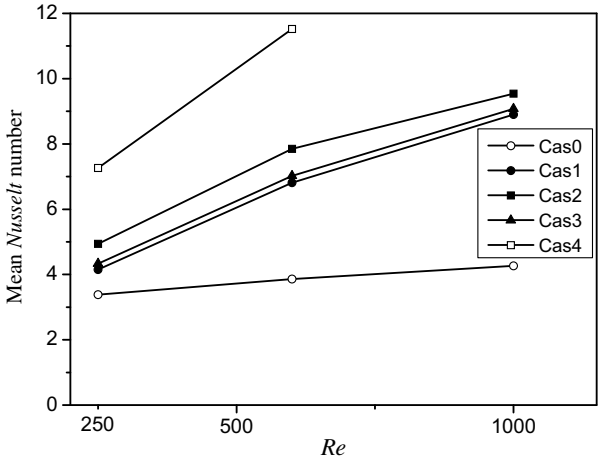

Fig. 10. Obstacle mean *Nusselt* number as function of *Re* for the five cases.

Table 3
Heat transfer rates for the four cases at different Reynolds numbers.

Case	Heat transfer enhancement (%)		
	$Re = 250$	$Re = 600$	$Re = 1000$
1	22.64	76.30	108.64
2	46.00	103.24	123.77
3	28.14	81.82	112.85
4	114.64	198.25	–

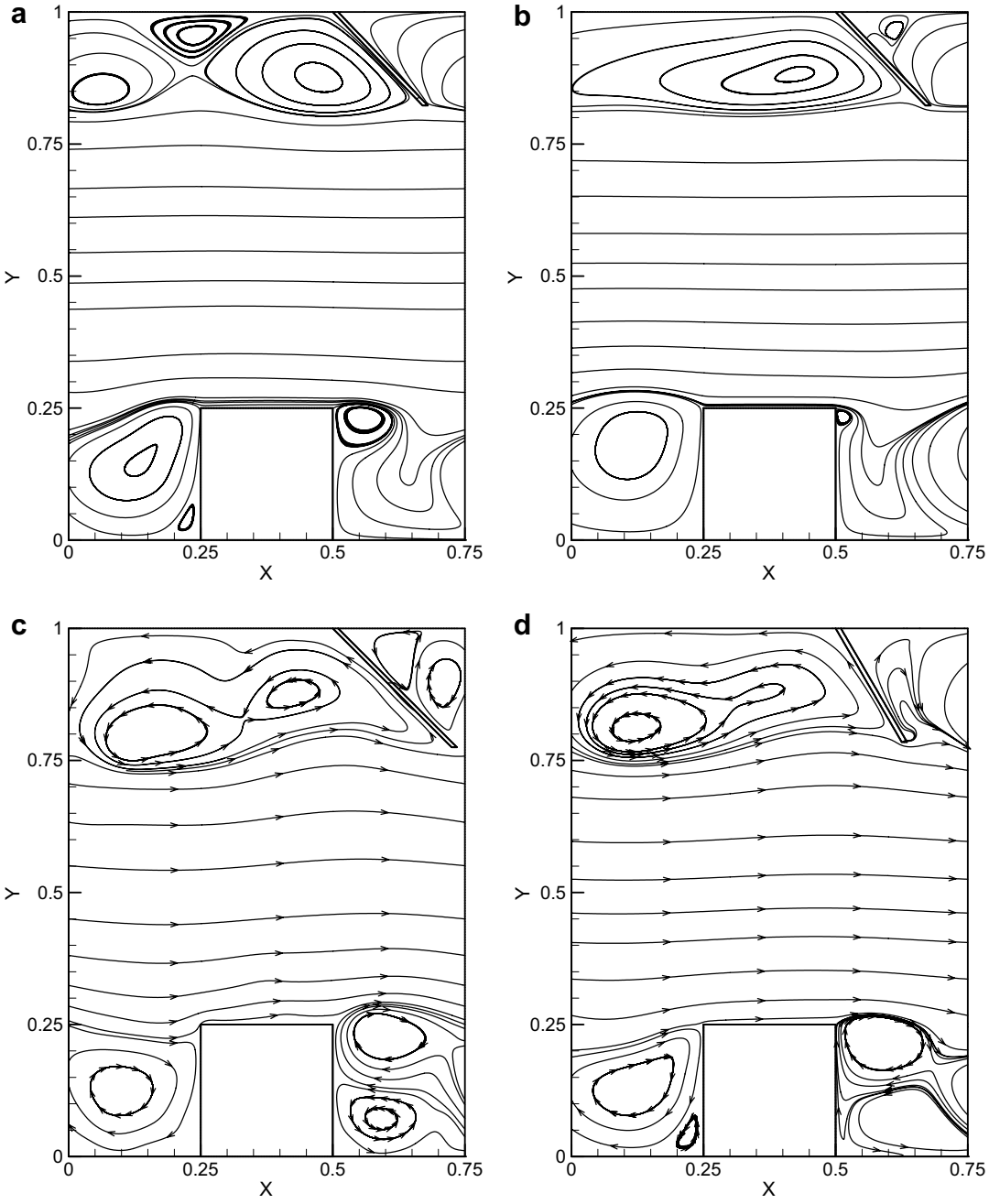

Fig. 11. Streamlines for case 1 at (a) $Re = 600$, (b) $Re = 1000$ and at $Re = 1000$ for (c) Case 2, and (d) case 3.

McGarry et al. [34] when using a curved vane as a heat transfer enhancement promoter.

For the other cases, a second counter-rotating recirculation zone appears behind the obstacle, in the vicinity of the lower corner (Fig. 11c and d). The presence of this second recirculation zone affects negatively the heat transfer. Moreover, a complex recirculation zone is observed for the third case, which retains longer the fluid in contact with the obstacle face and leads to increase its temperature.

5. Conclusions

Numerical simulations of fluid flow and conjugate heat transfer in a horizontal channel with periodically mounted obstacles on the lower wall and oblique plates as vortex generators at the upper one were performed for $250 \leqslant Re \leqslant 1000$. This paper highlights more specifically the enhancement of heat transfer by modifying the direction of the flow towards the obstacle faces to be cooled and by activating the self-oscillations using oblique plates placed periodically. It seems that this latter method can be considered as a new contribution in this research area. Various physical arrangements have been considered as plate length, oblique plate tilt angle and Reynolds number in order to investigate their influence on the thermal and flow characteristics in the steady state as well as in the self-sustained oscillatory flow. The analysis of the flow features clearly demonstrates the wavy periodic nature of the flow as it moves downstream, and show a vertical flow pattern of several vortices of different sizes, which increase and decrease in size. This phenomenon ejects the fluid from the cavity to the main flow. Because the thermal boundary is disturbed with flow oscillation,

numerical isotherms seem to follow the oscillatory flow behaviour. From the heat transfer viewpoint, the presence of vortex generators at the upper surface is a powerful mean to enhance the heat transfer compared to the basic grooved channel. For example, the heat transfer is found to enhance up 200% for $Re = 600$ and for a given geometric configuration of the oblique plate.

References

[1] H.W. Wu, S.W. Perng, Effect of oblique plate in heat transfer enhancement of mixed convection over heated blocks in horizontal channel, Int. J. Heat Mass Transfer 42 (1999) 1217.

[2] S.V. Garimella, P.A. Eibeck, Heat transfer characteristics of an array of protruding elements in single phase forced convection, Int. J. Heat Mass Transfer 33 (1990) 2659.

[3] C. Herman, E. Kang, Heat transfer enhancement in a grooved channel with curved vanes, Int. J. Heat Mass Transfer 45 (2002) 3741.

[4] S.-J. Yang, A numerical investigation of heat transfer enhancement for electronic devices using an oscillating vortex generator, Numer. Heat Transfer A 42 (2002) 269.

[5] W.-S. Fu, B.-H. Tong, Numerical investigation of heat transfer characteristics of the heated blocks in the channel with a transversely oscillating cylinder, Int. J. Heat Mass Transfer 47 (2004) 341.

[6] K.-H. Ko, N.K. Anand, Use of porous baffles to enhance heat transfer in a rectangular channel, Int. J. Heat Mass Transfer 46 (2003) 4191.

[7] C.H. Amon, D. Majumdar, C.V. Herman, F. Mayinger, B.B. Mikic, D.P. Sekulic, Numerical and experimental studies of self-sustained oscillatory flows in communicating channels, Int. J. Heat Mass Transfer 35 (1992) 3115.

[8] J.S. Nigen, C.H. Amon, Effect of material composition and localized heat generation on time-dependent conjugate heat transport, Int. J. Heat Mass Transfer 38 (1995) 1565.

[9] T. Nishimura, N. Oka, Y. Yoshinaka, K. Kunitsugu, Influence of imposed oscillatory frequency on mass transfer enhancement of grooved channels for pulsatile flow, Int. J Heat Mass Transfer 43 (2000) 2365.

[10] T. Adachi, H. Uehara, Correlation between heat transfer and pressure drop in channels with periodically grooved parts, Int. J. Heat Mass Transfer 44 (2001) 4333.

[11] A.M. Guzmán, M. Del Valle, Heat transfer enhancement in grooved channels due to flow bifurcations, Heat Mass Transfer 42 (2006) 967.

[12] Q. Wang, Y. Jaluria, Unsteady mixed convection in a horizontal channel with protruding heated blocks and a rectangular vortex promoter, Phys. Fluids 14 (2002) 2113.

[13] T. Nishimura, K. Kunitsugu, H. Nakagiri, Fluid mixing and local mass transfer characteristics in a grooved channel for self sustained oscillatory flow, Heat Transfer Jpn. Res. 27 (1998) 522.

[14] T. Howes, P.J. Shardlow, Simulation of mixing in unsteady flow through a periodically obstructed channel, Chem. Eng. Sci. 52 (1997) 1215.

[15] A.M. Anderson, R.J. Moffat, The adiabatic heat transfer coefficient and the superposition Kernel function. Part 1: Data for arrays of flatpacks for different flow conditions, Trans. ASME J. Electron. Pack. 114 (1992) 14.

[16] S.V. Patankar, C.H. Liu, E.M. Sparrow, Fully developed flow and heat transfer in ducts having streamwise-periodic variations of cross-sectional area, ASME J. Heat Transfer 99 (1977) 180.

[17] T. Adachi, H. Uehara, Linear stability analysis of flow in a periodically grooved channel, Int. J. Numer. Methods Fluids 41 (2003) 601.

[18] T. Adachi, S. Hasegawa, Transition of the flow in a symmetric channel with periodically expanded grooves, Chem. Eng. Sci. 61 (2006) 2721.

[19] K.M. Kelkar, S.V. Patankar, Numerical prediction of flow and heat transfer in a parallel plate channel with staggered fin, J. Heat Transfer 109 (1987) 25.

[20] T. Adachi, H. Uehara, Transitions and pressure drop characteristics of flow in channels with periodically grooved parts, JSME Int. J. B 44 (2001) 221.

[21] T.J. Young, K. Vafai, Convective flow and heat transfer in a channel containing multiple heated obstacles, Int. J. Heat Mass Transfer 41 (1998) 3279.

[22] B.A. Jubran, S.A. Swiety, M.A. Hamdan, Conjugate heat transfer and pressure drop characteristics of various array configurations to simulate the cooling of electronic modules, Int. J. Heat Mass Transfer 39 (1996) 3519.

[23] M. Yongmann, P.G. Tucker, Assessment of periodic flow assumption for unsteady heat transfer in grooved channels, ASME J. Heat Transfer 126 (2004) 1044.

[24] M. Greiner, An experimental investigation of resonant heat transfer enhancement in grooved channels, Int. J. Heat Mass Transfer 34 (1991) 1383.

[25] S. Lorenz, D. Mukomilow, W. Leiner, Distribution of heat transfer coefficient in a channel with periodic transverses grooves, Exp. Therm. Fluid Sci. 11 (1995) 234.

[26] M.A. Habib, A.M. Mobarak, M.A. Sallak, E.A. Adel Hadi, R.I. Affify, Experimental investigation oh heat transfer and flow over baffles of different heights, ASME J. Heat Transfer 116 (1994) 363.

[27] A. Grosse-Gorgemann, D. Weber, M. Fiebig, Experimental and numerical investigation of self-sustained oscillations in channels with periodic structures, Exp. Therm. Fluid Sci. 11 (1995) 226.

[28] S.V. Patankar, 1980, Numerical Heat Transfer And Fluid Flow, Hemisphere, New York.

[29] X. Chen, P. Han, A note on the solution of conjugate heat transfer problems using SIMPLE-like algorithms, Int. J. Heat Fluid Flow 21 (2000) 463.

[30] A. Korichi, Etude du transfert de chaleur lors d'un écoulement autour d'obstacles, Ph.D. Thesis, 03/2006, D/C.I, USTHB Alger, 2006.

[31] A. Korichi, L. Oufer, Numerical heat transfer in a rectangular channel with mounted obstacles on the upper and lower walls, Int. J. Therm. Sci. 44 (2005) 644.

[32] A. Korichi, L. Oufer, Unsteady heat transfer and pressure drop in channels with upper and lower walls mounted obstacles, Numer. Heat Transfer A 48 (2005) 711.

[33] A. Korichi, L. Oufer, Heat transfer enhancement in oscillatory flow in channel with periodically upper and lower walls mounted obstacles, Int. J. Heat Fluid Flow 28 (2007) 1003.

[34] M.M. Mcgarry, A. Campo, L.D. Hitt, Numerical simulations of heat and fluid flow in grooved channels with curved vanes, Numer. Heat Transfer A 46 (2004) 41.